Research Square

Preprints are preliminary reports that have not undergone peer review. They should not be considered conclusive, used to inform clinical practice, or referenced by the media as validated information.

Dynamic adsorption and regeneration of gaseous ammonia on oxalic acid-modified corn-straw biochar

Minghong Han
Harbin University of Science and Technology

Fen Li
hgxylf@126.com

Harbin University of Science and Technology

Huiyu Chen
Harbin University of Science and Technology

Hong Yan
Harbin University of Science and Technology

Dongdong Yang
Harbin University of Science and Technology

Zhichao Xing
Harbin University of Science and Technology

Jiaqi Li
Harbin University of Science and Technology

Research Article

Keywords: oxalic acid modification, biochar, adsorption, ammonia, regeneration

Posted Date: October 15th, 2026

DOI: https://doi.org/10.21203/rs.3.rs-11116595/v1

License: This work is licensed under a Creative Commons Attribution 4.0 International License. Read Full License

Additional Declarations: No competing interests reported.

Abstract

Oxalic acid modification was investigated as a simple route to improve gaseous ammonia (NH_3) adsorption by corn-straw biochar. A three-factor, four-level orthogonal design was used to screen pyrolysis temperature, holding time and oxalic acid concentration, after which the best-performing sample was tested for solvent regeneration. Among the 16 preparation conditions, CC-0.4-500-4, produced at 500°C for 4 h and treated with 0.4 mol L^{-1} oxalic acid, gave the highest observed NH_3 adsorption capacity of 27.56 mg g^{-1}. The material was predominantly mesoporous, with a BET surface area of 27.35 m^2 g^{-1} and carboxyl- and carbonyl-related surface structures. Changes in N_2-accessible pore volume and surface oxygen components after adsorption were consistent with pore-assisted transport and interactions between NH_3 and oxygen-containing sites. The post-adsorption N 1s spectrum also showed an increase in a nitrate-related component. An EPR signal at g = 2.0027 indicated persistent free radicals that may influence the local surface reactivity. A 10-min ethanol wash restored 67.6% of the initial adsorption capacity, and 44.5% remained after two regeneration cycles. The results show that oxalic acid-modified corn-straw biochar is a candidate adsorbent for dynamic NH_3 capture with solvent-assisted reuse.

1. Introduction

Ammonia (NH_3) is an important atmospheric pollutant because it contributes to secondary particulate matter formation and nitrogen deposition. Agriculture is the main global source, particularly through livestock-waste decomposition and the volatilisation of nitrogen fertilisers. Fossil-fuel combustion, biomass use, industrial production and waste treatment provide additional emissions (Crippa et al. 2018; Streets et al. 2003; Sutton et al. 2000; Van Damme et al. 2021). In the atmosphere, NH_3 reacts with acidic species to form ammonium sulfate and ammonium nitrate, contributing to $PM_{2.5}$ pollution. The resulting nitrogen deposition is also associated with soil acidification, aquatic eutrophication and adverse respiratory effects (Wu et al. 2008).

Available NH_3-control methods include absorption (Gonzalez-Salgado et al. 2023), adsorption (Adam et al. 2021), biological treatment (Song et al. 2024), catalytic decomposition (Santra et al. 2002) and plasma-based processes (Yi et al. 2019). Absorption produces a liquid stream that requires further treatment, whereas biological processes depend strongly on operating conditions. Catalytic and plasma-based methods may also require substantial energy input (Yang et al. 2025). Adsorption is comparatively simple and can be applied at low NH_3 concentrations, but its usefulness depends on adsorption capacity and regeneration performance.

Biochar is widely studied as an adsorbent because its feedstocks are abundant and its surface chemistry can be adjusted (Wen et al. 2023). Pristine biochar, however, may have poorly developed pores and relatively few active surface sites, which can restrict NH_3 uptake (Lete et al. 2026). Activation or chemical treatment can alter both pore structure and surface chemistry. Carboxyl, carbonyl and other

oxygen-containing groups are particularly relevant to NH_3 adsorption (Barin et al. 2017; Park and Jin 2005). Oxalic acid treatment has been used to modify carbonaceous adsorbents and increase carboxyl- and carbonyl-related structures (Tang et al. 2023), but most applications have concerned aqueous pollutants. Its effect on gaseous NH_3 capture, especially after adsorbent regeneration, has received less attention.

This study examined whether oxalic acid treatment could improve dynamic NH_3 adsorption by corn-straw biochar while retaining the possibility of solvent regeneration. An orthogonal design was used to screen the preparation conditions. The selected material was then characterised to relate its adsorption behaviour to pore structure and surface chemistry. Water and ethanol washing were compared as mild regeneration methods.

2. Materials and methods

2.1. Preparation of biochar

Clean, dry corn straw was cut into 1–2 cm pieces, ground and passed through a 60-mesh sieve. The sieved powder was stored in sealed containers. For pyrolysis, 2 g of powder was placed in a tubular furnace and heated under high-purity N_2 (≥ 99.99%, 100 mL min^{-1}) at 10 ℃ min^{-1} to 400, 500, 600 or 700°C. The target temperature was maintained for 2, 3, 4 or 5 h. Samples were then cooled to room temperature under continuous N_2 flow. The pristine biochars were labelled C-X-Y, where X is the pyrolysis temperature (℃) and Y is the holding time (h).

2.2. Oxalic acid modification of biochar

As shown in Fig. 1, 1.5 g of pristine biochar was immersed in 0.1, 0.2, 0.3 or 0.4 mol L^{-1} oxalic acid solution ($H_2C_2O_4$, analytical grade; Tianjin Kaitong Chemical Reagent Co., Ltd., China) and stirred for 12 h. The mixture was vacuum-filtered, and the solid was washed repeatedly with deionised water until the filtrate reached neutral pH. The product was dried at 80 ℃ for 24 h to constant mass. Modified biochars were labelled CC-Z-X-Y, where Z is the oxalic acid concentration and X and Y are the pyrolysis temperature and holding time of the precursor biochar.

2.3. NH_3 adsorption performance test

The fixed-bed system used for NH_3 adsorption is shown in Fig. 2. A stream containing 500 ppm NH_3 in N_2 was passed through a U-shaped acrylic reactor containing modified biochar at 20 mL min^{-1}. After the system had been checked for leaks, the outlet NH_3 concentration was monitored continuously with an ammonia detector. Breakthrough time was defined as the interval between the start of gas flow and an outlet concentration of 10 ppm. This value is 2% of the nominal inlet concentration and was used as a comparative threshold for this apparatus.

The NH_3 adsorption capacity of the biomass-derived biochar was calculated from the experimental data using Eq. (1):

$$\mathrm{q} = \int_0^t (1 - C_{out}/C_{in})dt * QC_{in}/M$$

1

where q is the NH_3 adsorption capacity (mg g^{-1}); Q is the volumetric flow rate of NH_3 (L min^{-1}); C_{in} and C_{out} are the inlet and outlet NH_3 concentrations (mg L^{-1}), respectively; M is the mass of oxalic acid-modified biochar (g); and t is the total NH_3 adsorption time (min).

2.4. Regeneration procedure

NH_3-saturated biochar was regenerated by water or ethanol washing. For water washing, spent biochar was immersed in distilled water and stirred at room temperature for 20, 30 or 40 min. For ethanol regeneration, the corresponding treatment times were 5, 10 and 15 min. After either treatment, the biochar was dried at 80 ℃ for 24 h, cooled to room temperature and stored in a sealed container.

2.5. Characterisation of biochar

Crystalline and turbostratic carbon features were examined by X-ray diffraction (XRD; Shimadzu, Japan), and surface morphology was observed by scanning electron microscopy (SEM; Apreo C, USA). Specific surface area and pore structure were measured with a Micromeritics ASAP 2460 analyser. N_2 adsorption-desorption isotherms were recorded at 77 K after vacuum degassing at 200 ℃ for 8 h. Surface chemical states were analysed by X-ray photoelectron spectroscopy (XPS; Shimadzu-Kratos AXIS Ultra DLD, Japan). Surface functional groups were examined by Fourier-transform infrared spectroscopy (FT-IR; Nicolet T60SX, USA). Raman spectra were collected with a Horiba LabRAM HR Evolution confocal Raman spectrometer.

3. Results and discussion

3.1. NH_3 adsorption performance

Pristine biochars were first prepared at 400–700 ℃ with holding times of 2–5 h (Supplementary Table S1). Although temperature and holding time can alter biochar composition (Suman and Gautam 2017), the samples in Fig. 3a showed similarly short breakthrough times. C-500-3 gave the longest response among the pristine materials, but its breakthrough time remained below 10 min.

Pyrolysis temperature, holding time and oxalic acid concentration were then evaluated at four levels in an $L_{16}(4^3)$ orthogonal design. Sixteen modified biochars were prepared, and NH_3 breakthrough time was

used as the response. The individual results are provided in Supplementary Table S2, and the corresponding range analysis is summarised in Table 1.

Every oxalic acid-modified sample had a longer NH_3 breakthrough time than C-500-3 (Supplementary Table S2). This improvement may be related to changes in pore structure and oxygen-containing surface components after treatment (Tang et al. 2023). CC-0.4-500-4 gave the longest breakthrough time (37 min), corresponding to an estimated adsorption capacity of 27.56 mg g^{-1}. The range values followed the order A (pyrolysis temperature) > C (oxalic acid concentration) > B (holding time). Within the tested design, pyrolysis temperature therefore showed the largest descriptive influence.

Table 1
Range analysis of the orthogonal-test results listed in Supplementary Table S2.

Parameter	Level	Factor		
		A	B	C
K_i	1	106	100	84
	2	121	100	108
	3	87	112	104
	4	91	93	109
$\bar{K}_i$	1	26.5	25	21
	2	30.3	25	27
	3	21.8	28	26
	4	22.8	23.3	27.3
Optimum level		A2	B3	C4
R		8.5	4.8	6.3
Order of influence		A > C > B		

The effect of pyrolysis temperature was examined further while holding time and oxalic acid concentration were fixed at 4 h and 0.4 mol L^{-1}, respectively. Breakthrough time first increased and then decreased between 400 and 700 °C, with the highest observed value at 500 °C (Fig. 3b).

The maximum at 500 °C may reflect a balance between pore development and the retention of reactive surface structures. Higher pyrolysis temperatures generally increase carbonisation and aromaticity while lowering the H and O contents of biochar (Al-Wabel et al. 2013; Ippolito et al. 2020). Loss of some

oxygen-containing groups at 600–700 ℃ may therefore have contributed to the shorter breakthrough times.

3.2. Characterisation of modified biochar

3.2.1. SEM analysis

The surface morphology of corn-straw biochar was examined by SEM, as shown in Fig. 4. C-500-3 retained the tubular channels of the straw fibres, with uneven and irregular pore walls (Fig. 4a, b). The tubular framework remained visible after oxalic acid treatment, although CC-0.4-500-4 contained more particulate deposits on the walls and within the channels (Fig. 4c, d). These morphological observations were considered together with the pore-structure, FT-IR and XPS results.

3.2.2. XRD and Raman analyses

The XRD patterns of C-500-3 and CC-0.4-500-4 are compared in Fig. 5a. Both samples showed a broad feature between 20° and 30°, centred near 23°, which is typical of the (002) stacking of low-crystallinity turbostratic carbon. The similar profiles show that oxalic acid treatment did not markedly alter the overall carbon framework.

CC-0.4-500-4 showed Raman D and G bands at 1351 and 1581 cm^{-1}, respectively (Fig. 5b). These bands arise from disordered carbon and vibrations of the sp^2 carbon framework. The I_D/I_G ratio of 0.75 indicates that ordered sp^2 domains coexisted with structural disorder (Zhang et al. 2024). The XRD and Raman data therefore show that the material retained a low-crystallinity carbon framework after modification. The accompanying changes in surface chemistry and pore structure were examined by FT-IR, XPS and N_2 adsorption-desorption analysis.

3.2.3. FT-IR analysis

The FT-IR spectra of C-500-3 and CC-0.4-500-4 are shown in Fig. 5c. Both materials had a broad band at 3300–3500 cm^{-1}, mainly associated with O-H stretching, with possible contributions from adsorbed water or N-H vibrations. The altered profile of CC-0.4-500-4 in this region indicates a change in hydroxyl-related surface structures after oxalic acid treatment.

Bands near 2930 and 2850 cm^{-1} were assigned to aliphatic C-H stretching. The region from 1560 to 1720 cm^{-1} contained C = O-related vibrations, whereas bands between 1070 and 1280 cm^{-1} were associated mainly with C-O and C-O-C groups (Chen et al. 2024). These oxygen-related bands were more pronounced in CC-0.4-500-4. The fitted C 1s and O 1s spectra also showed changes in carboxyl-, carbonyl- and C-O-related surface components.

Oxalic acid treatment therefore changed the oxygen-containing structures at the biochar surface. These sites may contribute to NH_3 adsorption through acid-base interactions and hydrogen bonding, in agreement with the XPS changes observed after adsorption.

3.2.4. XPS analysis

XPS was used to compare the surface chemistry of C-500-3 and CC-0.4-500-4 and to examine CC-0.4-500-4 before and after NH_3 adsorption. The survey spectra contained predominantly C and O, together with a small N signal (Fig. 5d).

The high-resolution C 1s spectra are shown in Fig. 6a and b. Both samples were dominated by the C-C/C = C component near 284.8 eV. For C-500-3, the broad component near 288.1 eV was assigned to overlapping oxygenated carbon species, with possible contributions from C = O and C-O structures. For CC-0.4-500-4, the components near 285.8 and 289.1 eV were tentatively assigned to C-O and O-C = O-related structures, respectively. Because oxygen-containing components in biochar may overlap, these assignments were considered together with the FT-IR and O 1s results (Chen et al. 2024). Overall, the spectra suggest that oxalic acid treatment altered the distribution of oxygenated carbon structures at the biochar surface.

The O 1s spectra before and after NH_3 adsorption are compared in Fig. 6c. Components near 531.8-531.9 and 533.4 eV were tentatively assigned to carbonyl oxygen and C-O/C-OH-related oxygen, respectively. After adsorption, the fitted C-O/C-OH contribution increased slightly, whereas the C = O contribution decreased slightly; the high-binding-energy oxygen component changed little (Supplementary Table S3). These modest shifts are consistent with a change in the local environment of oxygen-containing surface groups.

The N 1s spectra also changed after NH_3 adsorption (Fig. 6d). An H-N-related component near 400.3 eV was present before and after adsorption, whereas the high-binding-energy component near 406.1 eV increased after exposure to NH_3. This region is commonly associated with nitrate-related species (Barroso-Bogeat et al. 2019). Previous studies have linked acidic oxygen-containing groups on biochar with gaseous NH_3 adsorption through Brønsted acid-base interactions (Ko and Ko 2026; Ro et al. 2015). The present spectra are therefore consistent with pore accommodation and surface acid-base interactions, accompanied by the possible formation or stabilisation of nitrate-related species.

3.2.5. Specific surface area and pore-structure analysis

Pore properties of CC-0.4-500-4 before and after NH_3 adsorption are given in Table 2 and Fig. 7. Before adsorption, the BET surface area was 27.3485 $m^2 g^{-1}$ and the total pore volume was 0.0226 $cm^3 g^{-1}$. Mesopores contributed 0.0187 $cm^3 g^{-1}$, or 82.74% of the total pore volume, and the main pore-size range was approximately 3–5 nm. This pore system can provide paths for NH_3 transport and space for local accumulation.

After NH_3 adsorption, the BET surface area and total pore volume decreased to 20.0419 $m^2 g^{-1}$ and 0.0179 $cm^3 g^{-1}$, respectively. The micropore and mesopore volumes also fell to 0.00101 and 0.0142 $cm^3 g^{-1}$. These changes are consistent with partial pore occupation or lower N_2 accessibility after

adsorption. The micropores and mesopores therefore appear to assist intraparticle transport and local NH_3 enrichment, while surface chemical sites also contribute to the measured capacity.

Table 2
BET specific surface area and pore-structure parameters of oxalic acid-modified biochar CC-0.4-500-4 before and after NH_3 adsorption.

Sample	State	BET surface area (m^2 g^{-1})	Total pore volume (cm^3 g^{-1})	Micropore volume (cm^3 g^{-1}) (fraction, x%)	Mesopore volume (cm^3 g^{-1}) (fraction, x%)	Macropore volume (cm^3 g^{-1}) (fraction, x%)
CC-0.4-500-4	Before adsorption	27.3485	0.0226	0.00171 (7.57%)	0.0187 (82.74%)	0.00217 (9.69%)
	After adsorption	20.0419	0.0179	0.00101 (5.64%)	0.0142 (79.33%)	0.00266 (15.03%)

The N_2 adsorption-desorption isotherm had type IV characteristics and a clear hysteresis loop (Fig. 7b), confirming a predominantly mesoporous structure with a small micropore fraction (Thommes et al. 2015). The pore network is suitable for NH_3 transport and physical accommodation. Considered with the FT-IR and XPS results, the data point to a combined contribution from pore-assisted transport and interactions at oxygen-containing surface sites.

3.3. Regeneration performance of oxalic acid-modified biochar

Regeneration can reduce adsorbent consumption and improve the practical value of biochar prepared from agricultural residues. Thermal regeneration can promote desorption but may also consume substantial energy and alter carbon pore structures (Dong et al. 2014; Vakili et al. 2024). Water and ethanol washing were therefore selected as mild treatments that could remove weakly bound NH_3 while limiting changes to the carbon framework.

Water readily dissolves NH_3 and has previously restored part of the adsorption capacity of NH_3-saturated biochar (Ro et al. 2015). Ethanol provides a different polar environment and was included to test the effect of solvent type. The recovery of CC-0.4-500-4 was compared after different washing times with each solvent.

3.3.1. NH_3 adsorption performance of regenerated oxalic acid-modified biochar

Water-washing results are shown in Fig. 8a. Adsorption first improved and then declined as the washing time increased from 20 to 40 min. The highest recovery occurred after 30 min, when the breakthrough time was 24 min and the adsorption capacity was 17.87 mg g^{-1}. This capacity was 64.6% of that of the fresh sample. After a second cycle under the same conditions, 41.5% of the initial capacity remained.

Ethanol regeneration produced breakthrough times of 23, 25 and 21 min after treatments of 5, 10 and 15 min, respectively (Fig. 8b). The corresponding capacities were 17.13, 18.62 and 15.64 mg g^{-1}. The highest value was obtained after 10 min, and the sample retained 44.5% of its initial capacity after a second cycle.

Both washing methods recovered a substantial fraction of the adsorption capacity. Ethanol treatment for 10 min gave a slightly higher recovery than water washing for 30 min, both after the first treatment and after the second cycle. The response to these mild treatments shows that part of the retained NH_3 can be released and the material can be reused.

3.3.2. Specific surface area and pore-structure analysis of regenerated oxalic acid-modified biochar

Pore properties after two regeneration cycles are summarised in Supplementary Table S4 and Fig. 9a and b. Both treatments lowered the BET surface area and total pore volume relative to the fresh material. After water and ethanol regeneration, the BET surface areas were 11.32 and 9.95 m^2 g^{-1}, respectively, while mesopores remained the dominant pore class.

After two ethanol cycles, the sample had lower BET surface area, total pore volume and mesopore volume than the water-washed sample, yet retained slightly more NH_3 adsorption capacity. This contrast shows that regeneration performance was not determined by pore volume or surface area alone and remained sensitive to surface composition.

Both regenerated samples retained type IV isotherms with hysteresis loops, indicating that mesopores remained dominant (Fig. 9c, d) (Thommes et al. 2015). N_2 uptake was generally higher after water washing than after ethanol treatment, consistent with the BET and total-pore-volume data. The continued uptake of the ethanol-regenerated sample at high relative pressure suggests the presence of larger pores or interparticle voids (Schlumberger and Thommes 2021).

3.3.3. XPS analysis of regenerated oxalic acid-modified biochar

XPS was used to examine the surface composition of CC-0.4-500-4 after water or ethanol regeneration (Fig. 10). C and O remained the main surface elements in the fresh and regenerated samples, with a smaller N contribution.

The C 1s spectra of both regenerated samples were dominated by the C-C/C = C component near 284.8 eV (Fig. 10c). C-O and C = O-related components were also resolved, showing that oxygenated carbon structures remained after regeneration.

C-O/C-OH-related components dominated the O 1s spectra of both regenerated samples, with a smaller C = O contribution (Fig. 10d). The relative C = O contribution was higher after water washing, whereas C-O/C-OH was more pronounced after ethanol treatment. An O-C = O related component was not resolved in either regenerated sample, indicating a shift in the distribution of surface oxygen components.

The N 1s spectra differed between the two regeneration methods (Fig. 10e). The water-washed sample was dominated by an H-N-related component near 400.4 eV, together with smaller C-N and other N-containing components. In the ethanol-regenerated sample, a high-binding-energy component near 408.0 eV had a larger fitted area and was tentatively assigned to nitrate-related species. An H-N-related component near 400.1 eV remained, whereas a distinct C-N contribution was not resolved. The fitted spectra therefore show that water and ethanol left different distributions of surface nitrogen species.

Capacity declined as the pore parameters and the distribution of oxygen-containing components changed over repeated cycles. Oxygen-containing groups can make a substantial contribution to gaseous NH_3 adsorption by biochar (Lete et al. 2026). The regeneration results are therefore consistent with contributions from both pore accessibility and surface chemistry.

3.4. Proposed mechanism of NH_3 adsorption by oxalic acid-modified biochar

The combined SEM, BET, FT-IR, XPS and EPR results support a working description of NH_3 capture by CC-0.4-500-4. The main contributions are pore-assisted transport and accommodation, interactions with oxygen-containing surface sites, and the possible formation of high-binding-energy nitrogen species. The proposed process is illustrated in Fig. 12.

The pore network provides transport paths into the particles and space for NH_3 near the pore walls. Mesopores accounted for 82.74% of the total pore volume, with a smaller micropore fraction. After adsorption, the lower BET surface area and pore volumes were consistent with partial pore occupation or reduced N_2 accessibility. The moderate BET surface area of 27.35 $m^2 g^{-1}$ also indicates that pore filling was not the only source of capacity. The pores probably contributed mainly to transport, local enrichment and physical adsorption.

Oxalic acid treatment also changed the oxygenated carbon structures at the surface. FT-IR and fitted C 1s and O 1s spectra showed C-O/C-OH, C = O and carboxyl-related components. These acidic sites can interact with NH_3 through Brønsted acid-base reactions and hydrogen bonding. After adsorption, the C-O/C-OH contribution increased from 69.95 to 71.10%, while C = O decreased from 23.37 to 22.26%. The shifts are consistent with the involvement of oxygen-containing sites during NH_3 capture.

The N 1s results provide additional information on retained surface species. The H-N-related component near 400.3 eV remained after adsorption, consistent with NH_3 retention in N-H-containing forms. The increase in the high-binding-energy component near 406.1 eV was tentatively associated with nitrate-related species. Part of the adsorbed NH_3 may therefore have been stabilised in higher-binding-energy nitrogen forms in the presence of surface oxygen sites.

CC-0.4-500-4 also showed a clear EPR signal at g = 2.0027, confirming the presence of persistent free radicals. Signals below g = 2.003 are generally associated with predominantly carbon-centred radicals in biochar (Yuan et al. 2022). Together with carbon defects and oxygen-containing structures, these radicals may affect the local electronic environment and participate in surface reactions during NH_3 capture (Xie et al. 2024).

The regeneration results are also consistent with contributions from pores and surface sites. Water and ethanol washing released part of the retained NH_3, while pore parameters and oxygen-containing components changed over repeated cycles. These changes accompanied the gradual decrease in capacity.

Overall, NH_3 capture by CC-0.4-500-4 is consistent with pore-assisted transport and accommodation combined with interactions at oxygen-containing surface sites. The XPS spectra also suggest that some adsorbed nitrogen was stabilised in high-binding-energy forms. Persistent free radicals may further influence the local surface reactivity.

4. Conclusions

Oxalic acid treatment improved the dynamic NH_3 adsorption of corn-straw biochar. Among the preparation conditions examined, CC-0.4-500-4 gave the highest observed capacity of 27.56 mg g^{-1} after pyrolysis at 500 °Cfor 4 h and treatment with 0.4 mol L^{-1} oxalic acid.

Pore-structure, FT-IR and XPS results indicate that NH_3 uptake involved pore-assisted transport and interactions with oxygen-containing surface sites. Changes in the N 1s spectrum were consistent with the possible stabilisation of nitrate-related species. The EPR signal at g = 2.0027 also showed that persistent radicals were present and may contribute to local surface reactions.

Water and ethanol washing recovered part of the adsorption capacity. A 10-min ethanol treatment restored 67.6% of the initial value, and 44.5% remained after two regeneration cycles. The response confirms that mild solvent treatment can release retained NH_3 and allow the material to be reused.

Within the tested conditions, oxalic acid-modified corn-straw biochar combined improved gaseous NH_3 adsorption with measurable solvent-regeneration performance. The material therefore provides a useful basis for developing adsorbents from agricultural residues for NH_3 pollution control.

Declarations

Declaration of competing interest

The authors declare that they have no known competing financial interests or personal relationships that could have appeared to influence the work reported in this paper.

Author Contribution

Minghong Han: Writing - original draft, Visualization. Fen Li: Funding acquisition. Huiyu Chen: Methodology. Hong Yan: Supervision. Dongdong Yang: Investigation. Zhichao Xing: Writing - review & editing. Jiaqi Li: Validation.

Acknowledgement

This work was supported by the National Natural Science Foundation of China (Grant No. 22278100).

Data Availability

All data supporting the findings of this study are available within the paper and its Supplementary Information.

CRediT authorship contribution statement

Minghong Han: Writing - original draft, Visualization. **Fen Li**: Funding acquisition. **Huiyu Chen**: Methodology. **Hong Yan**: Supervision. **Dongdong Yang**: Investigation. **Zhichao Xing**: Writing - review & editing. **Jiaqi Li**: Validation.

References

1. Crippa, M., Guizzardi, D., Muntean, M., Schaaf, E., Dentener, F., Van Aardenne, J. A., et al. (2018, April 9). Gridded emissions of air pollutants for the period 1970–2012 withinEDGAR v4.3.2. Data, Algorithms, and Models. https://doi.org/10.5194/essd-2018-31
2. Streets, D. G., Bond, T. C., Carmichael, G. R., Fernandes, S. D., Fu, Q., He, D., et al. (2003). An inventory of gaseous and primary aerosol emissions in Asia in the year 2000. *Journal of Geophysical Research: Atmospheres*, 108(D21), 2002JD003093. https://doi.org/10.1029/2002JD003093
3. Sutton, M. A., Dragosits, U., Tang, Y. S., & Fowler, D. (2000). Ammonia emissions from non-agricultural sources in the UK. Atmospheric Environment, 34(6), 855–869.

https://doi.org/10.1016/S1352-2310(99)00362-3

4. Van Damme, M., Clarisse, L., Franco, B., Sutton, M. A., Erisman, J. W., Wichink Kruit, R., et al. (2021). Global, regional and national trends of atmospheric ammonia derived from a decadal (2008–2018) satellite record. Environmental Research Letters, 16(5), 55017. https://doi.org/10.1088/1748-9326/abd5e0
5. Wu, S.-Y., Hu, J.-L., Zhang, Y., & Aneja, V. P. (2008). Modeling atmospheric transport and fate of ammonia in north carolina—part II: effect of ammonia emissions on fine particulate matter formation. Atmospheric Environment, 42(14), 3437–3451. https://doi.org/10.1016/j.atmosenv.2007.04.022
6. Gonzalez-Salgado, I., Bounouba, M., Dubos, S., Mengelle, E., Guigui, C., & Sperandio, M. (2023). Influence of feed salinity on ammonia recovery from high-strength effluents in transmembrane chemical absorption process. Journal of Membrane Science, 687, 122086. https://doi.org/10.1016/j.memsci.2023.122086
7. Adam, M. R., Othman, M. H. D., Sheikh Abdul Kadir, S. H., Puteh, M. H., Jamalludin, M. R., Md Nordin, N. A. H., et al. (2021). Fabrication, performance evaluation, and optimisation of adsorptive ammonia removal using hollow fibre ceramic membrane: response surface methodology approach. Microporous and Mesoporous Materials, 316, 110932. https://doi.org/10.1016/j.micromeso.2021.110932
8. Song, Z., Hao, S., Zhang, L., Fan, X., & Peng, Y. (2024). High-rate nitrogen removal by partial nitritation/anammox with a single-stage membrane-aerated biofilm reactor. Journal of Environmental Management, 349, 119581. https://doi.org/10.1016/j.jenvman.2023.119581
9. Santra, A. K., Min, B. K., Yi, C. W., Luo, K., Choudhary, T. V., & Goodman, D. W. (2002). Decomposition of NH_3 on Ir(100): a temperature programmed desorption study. *Journal of Physical Chemistry B*, *106*(2), 340–344. https://doi.org/10.1021/jp0123132
10. Yi, Y., Wang, L., Guo, Y., Sun, S., & Guo, H. (2019). Plasma-assisted ammonia decomposition over Fe–Ni alloy catalysts for CO_x-free hydrogen. *AIChE Journal*, *65*(2), 691–701. https://doi.org/10.1002/aic.16479
11. Yang, Y. Chen, H. Li, F. Yu, C. Ai, H. Li, Q. Zhen, M. (2025). Research progress of highly efficient ammonia adsorption materials in waste gas. *Journal of Harbin University of Science and Technology*, *30*(3), 148–158. https://doi.org/10.15938/j.jhust.2025.03.017
12. Wen, C., Liu, T., Wang, D., Wang, Y., Chen, H., Luo, G., et al. (2023). Biochar as the effective adsorbent to combustion gaseous pollutants: preparation, activation, functionalization and the adsorption mechanisms. Progress in Energy and Combustion Science, 99, 101098. https://doi.org/10.1016/j.pecs.2023.101098
13. Lete, A., Navarro-Gil, Á., Millera, Á., Fonts, I., Ceamanos, J., Gil-Lalaguna, N., & Gea, G. (2026). Rice husk pristine biochar for dynamic gas-phase NH3 adsorption: impact of pyrolysis temperature and mechanism. Chemical Engineering Science, 334, 124313. https://doi.org/10.1016/j.ces.2026.124313

14. Barin, G., Peterson, G. W., Crocellà, V., Xu, J., Colwell, K. A., Nandy, A., et al. (2017). Highly effective ammonia removal in a series of brønsted acidic porous polymers: investigation of chemical and structural variations. Chemical Science, 8(6), 4399–4409. https://doi.org/10.1039/C6SC05079D
15. Park, S.-J., & Jin, S.-Y. (2005). Effect of ozone treatment on ammonia removal of activated carbons. Journal of Colloid and Interface Science, 286(1), 417–419. https://doi.org/10.1016/j.jcis.2005.01.043
16. Tang, X., Lei, Y., Yu, C., Wang, C., Zhang, P., & Lu, H. (2023). Highly-efficient degradation of organic pollutants by oxalic acid modified sludge biochar: mechanism and pathways. Chemosphere, 325, 138409. https://doi.org/10.1016/j.chemosphere.2023.138409
17. Suman, S., & Gautam, S. (2017). Effect of pyrolysis time and temperature on the characterization of biochars derived from biomass. Energy Sources, Part A: Recovery, Utilization, and Environmental Effects, 39(9), 933–940. https://doi.org/10.1080/15567036.2016.1276650
18. Al-Wabel, M. I., Al-Omran, A., El-Naggar, A. H., Nadeem, M., & Usman, A. R. A. (2013). Pyrolysis temperature induced changes in characteristics and chemical composition of biochar produced from conocarpus wastes. Bioresource Technology, 131, 374–379. https://doi.org/10.1016/j.biortech.2012.12.165
19. Ippolito, J. A., Cui, L., Kammann, C., Wrage-Mönnig, N., Estavillo, J. M., Fuertes-Mendizabal, T., et al. (2020). Feedstock choice, pyrolysis temperature and type influence biochar characteristics: a comprehensive meta-data analysis review. Biochar, 2(4), 421–438. https://doi.org/10.1007/s42773-020-00067-x
20. Zhang, S., Jia, X., Wang, X., Chen, J., Cheng, C., Jia, X., & Hu, H. (2024). Using the conditional process analysis model to characterize the evolution of carbon structure in taxodium ascendens biochar with varied pyrolysis temperature and holding time. Plants, 13(3), 460. https://doi.org/10.3390/plants13030460
21. Chen, J., Zhou, J., Zheng, W., Leng, S., Ai, Z., Zhang, W., et al. (2024). A complete review on the oxygen-containing functional groups of biochar: formation mechanisms, detection methods, engineering, and applications. Science of The Total Environment, 946, 174081. https://doi.org/10.1016/j.scitotenv.2024.174081
22. Barroso-Bogeat, A., Alexandre-Franco, M., Fernández-González, C., & Gómez-Serrano, V. (2019). Activated carbon surface chemistry: changes upon impregnation with al(III), fe(III) and zn(II)-metal oxide catalyst precursors from NO3- aqueous solutions. Arabian Journal of Chemistry, 12(8), 3963–3976. https://doi.org/10.1016/j.arabjc.2016.02.018
23. Ro, K., Lima, I., Reddy, G., Jackson, M., & Gao, B. (2015). Removing gaseous NH3 using biochar as an adsorbent. Agriculture, 5(4), 991–1002. https://doi.org/10.3390/agriculture5040991
24. Ko, M., & Ko, J. H. (2026). Synergistic adsorption of NH3 and H2S over layered hydrochar-derived pyrochars: mechanistic divergence and cooperative acid-base activation. Scientific Reports, 16(1), 13860. https://doi.org/10.1038/s41598-026-43340-y

25. Thommes, M., Kaneko, K., Neimark, A. V., Olivier, J. P., Rodriguez-Reinoso, F., Rouquerol, J., & Sing, K. S. W. (2015). Physisorption of gases, with special reference to the evaluation of surface area and pore size distribution (IUPAC technical report). Pure and Applied Chemistry, 87(9–10), 1051–1069. https://doi.org/10.1515/pac-2014-1117
26. Vakili, M., Cagnetta, G., Deng, S., Wang, W., Gholami, Z., Gholami, F., et al. (2024). Regeneration of exhausted adsorbents after PFAS adsorption: a critical review. Journal of Hazardous Materials, 471, 134429. https://doi.org/10.1016/j.jhazmat.2024.134429
27. Dong, L., Liu, W., Jiang, R., & Wang, Z. (2014). Physicochemical and porosity characteristics of thermally regenerated activated carbon polluted with biological activated carbon process. Bioresource Technology, 171, 260–264. https://doi.org/10.1016/j.biortech.2014.08.067
28. Schlumberger, C., & Thommes, M. (2021). Characterization of hierarchically ordered porous materials by physisorption and Mercury porosimetry—a tutorial review. Advanced Materials Interfaces, 8(4), 2002181. https://doi.org/10.1002/admi.202002181
29. Yuan, J., Wen, Y., Dionysiou, D. D., Sharma, V. K., & Ma, X. (2022). Biochar as a novel carbon-negative electron source and mediator: electron exchange capacity (EEC) and environmentally persistent free radicals (EPFRs): a review. Chemical Engineering Journal, 429, 132313. https://doi.org/10.1016/j.cej.2021.132313
30. Xie, J., Latif, J., Yang, K., Wang, Z., Zhu, L., Yang, H., et al. (2024). A state-of-art review on the redox activity of persistent free radicals in biochar. Water Research, 255, 121516. https://doi.org/10.1016/j.watres.2024.121516

Figures

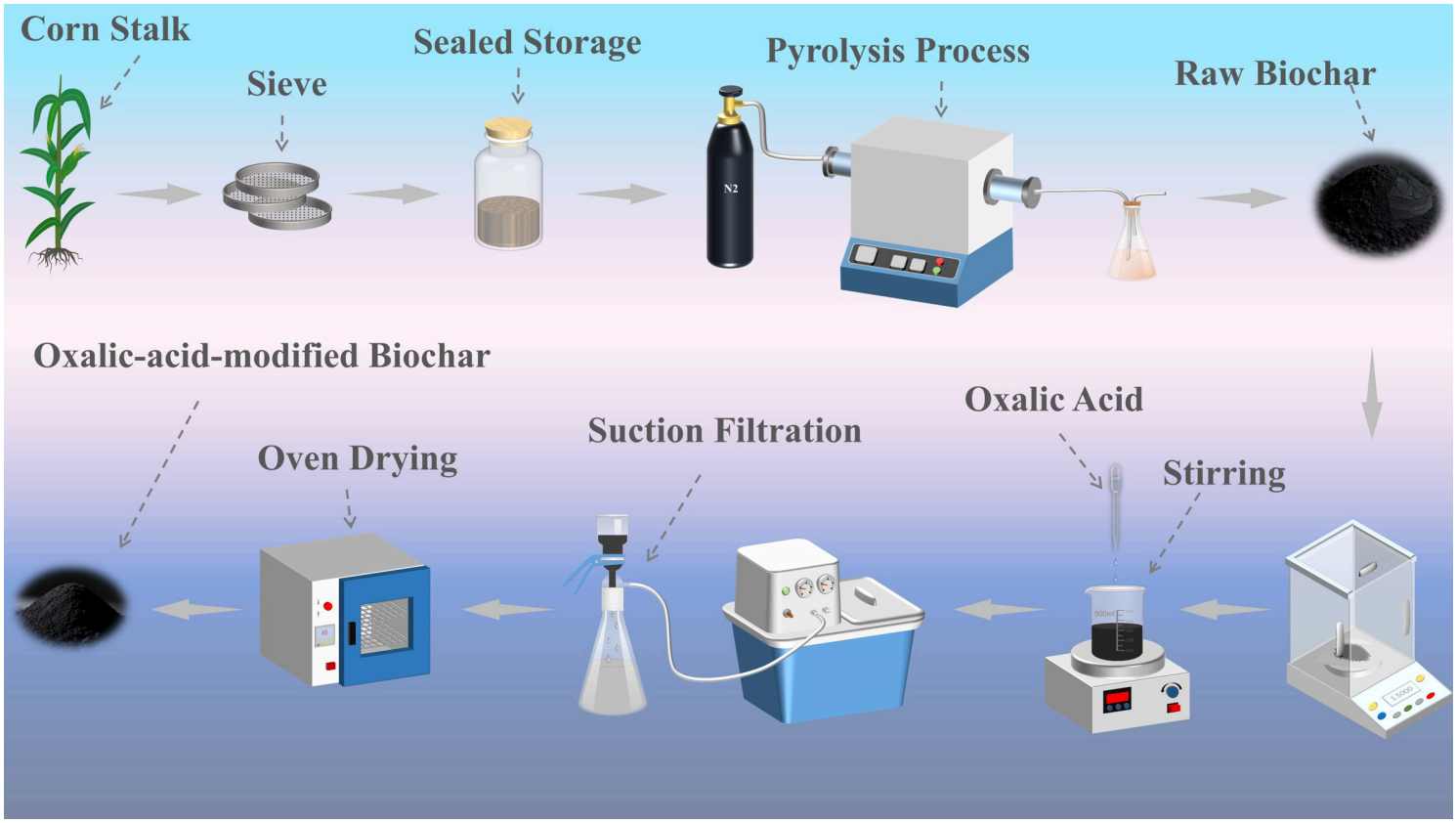

Figure 1

Experimental procedure for oxalic acid modification of biochar.

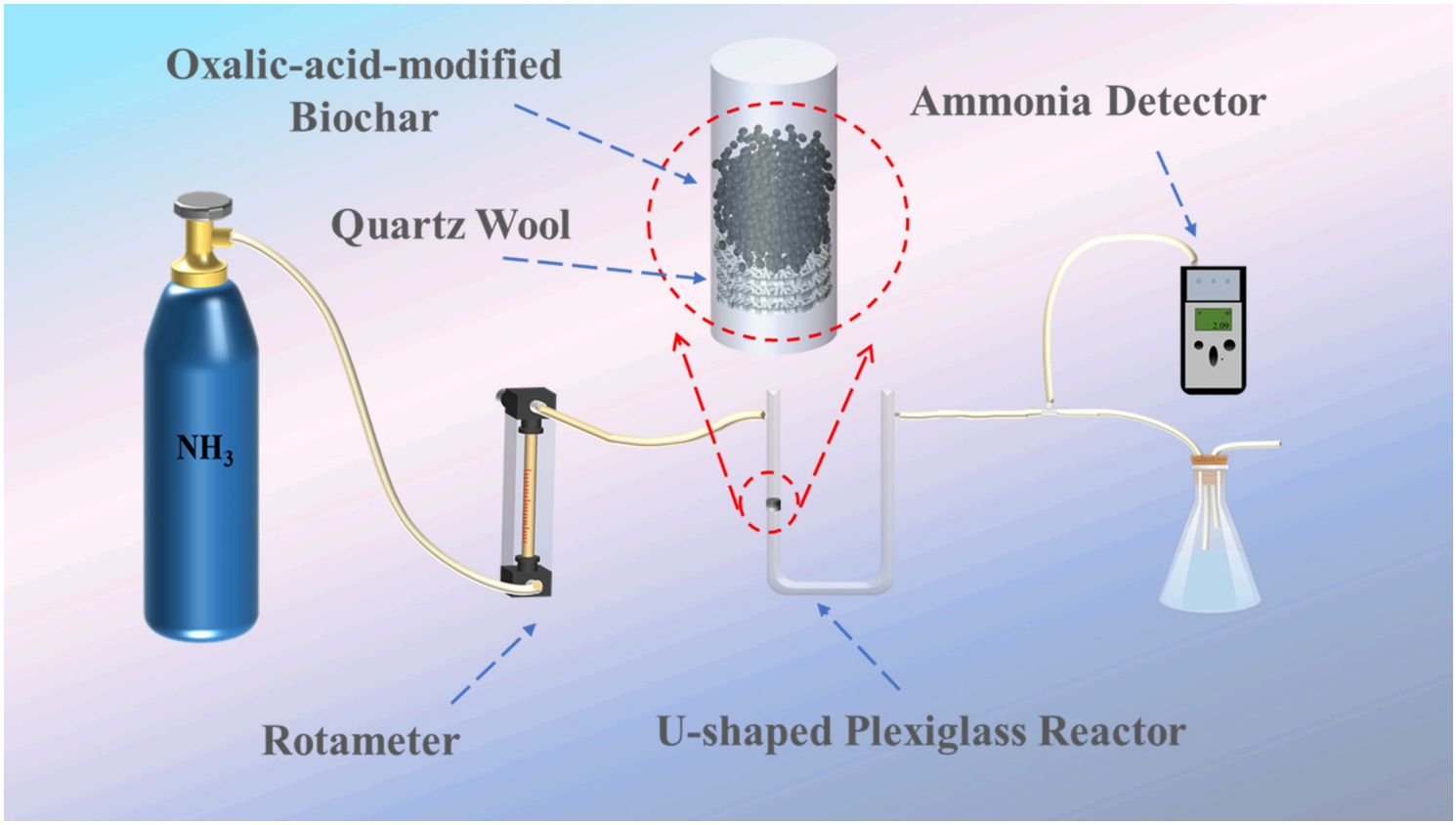

Figure 2

Apparatus used to evaluate NH_3 adsorption performance.

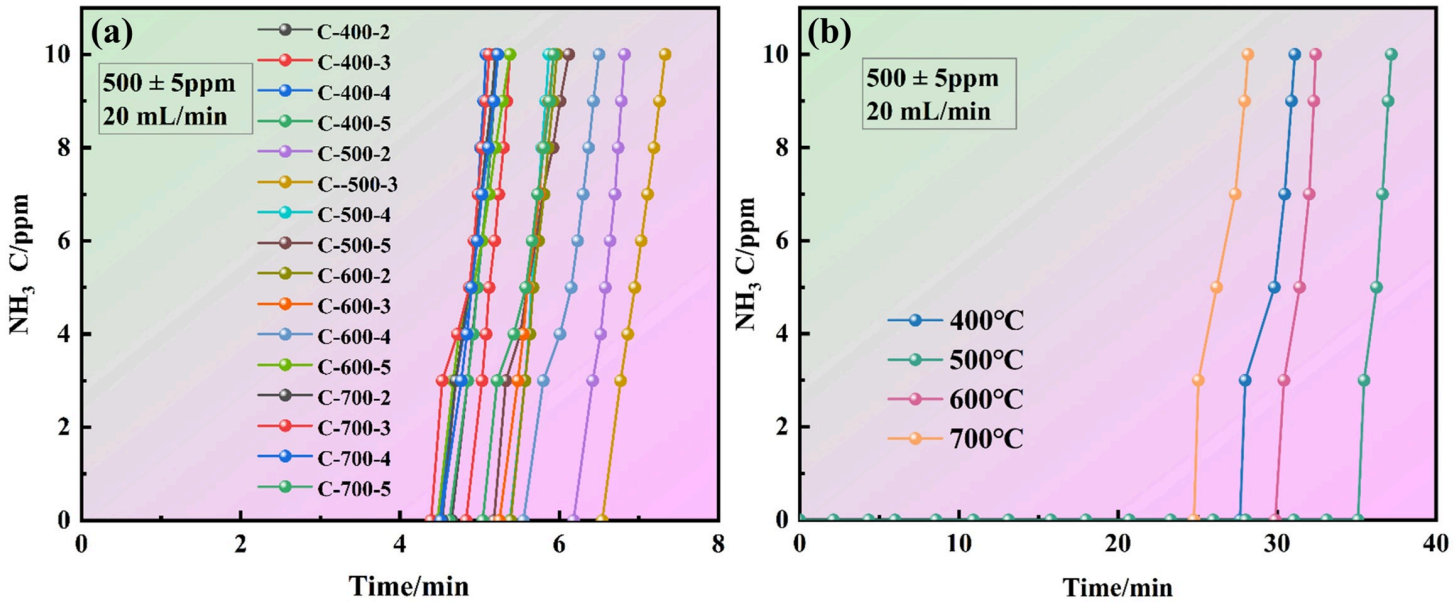

Figure 3

NH_3 adsorption-time profiles of (a) pristine biochars prepared under different conditions and (b) oxalic acid-modified biochars prepared at different pyrolysis temperatures (fixed pyrolysis time, 4 h; oxalic acid concentration, 0.4 mol L^{-1})

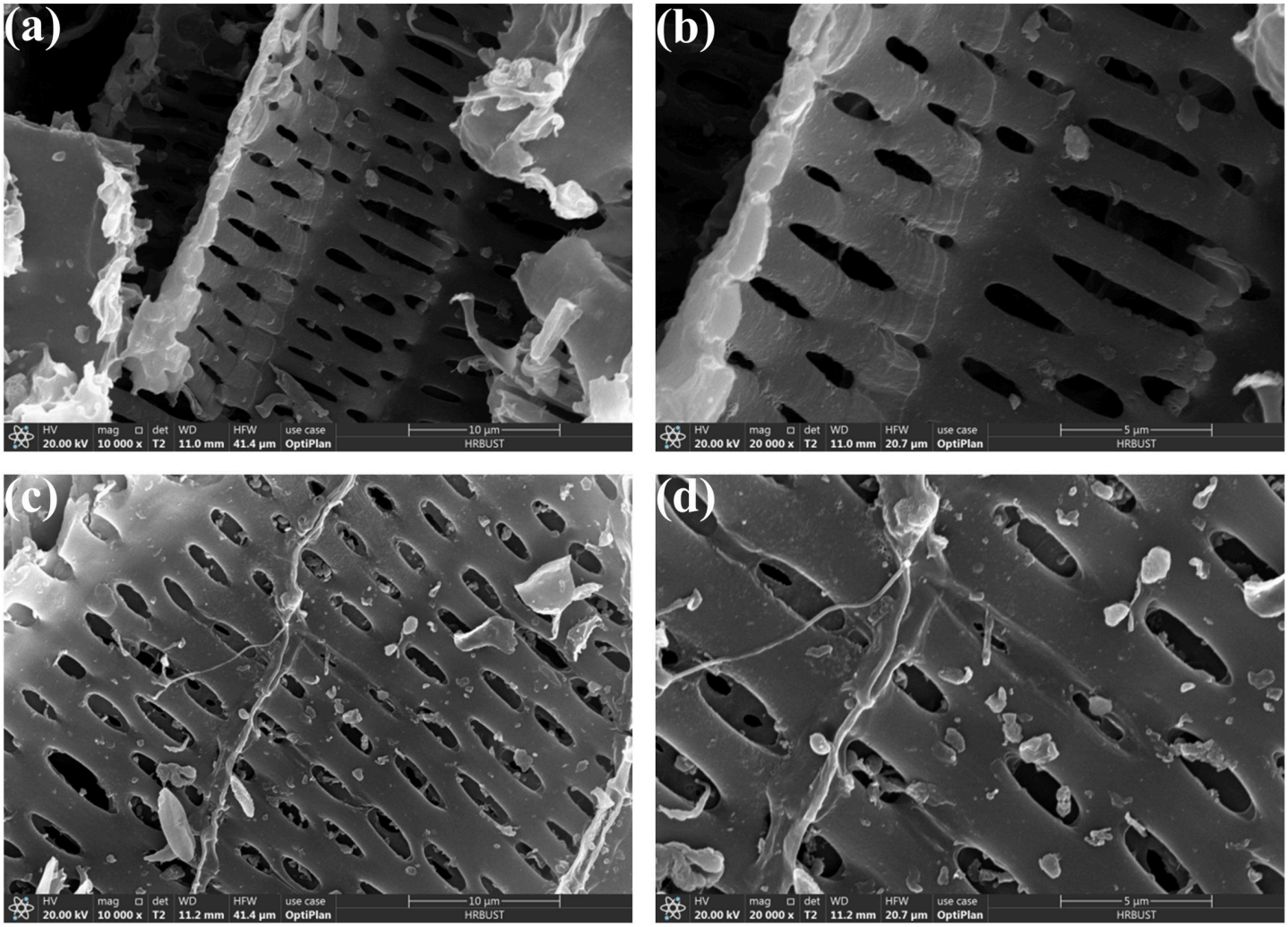

Figure 4

SEM images of pristine and oxalic acid-modified biochars: (a, b) C-500-3 and (c, d) CC-0.4-500-4.

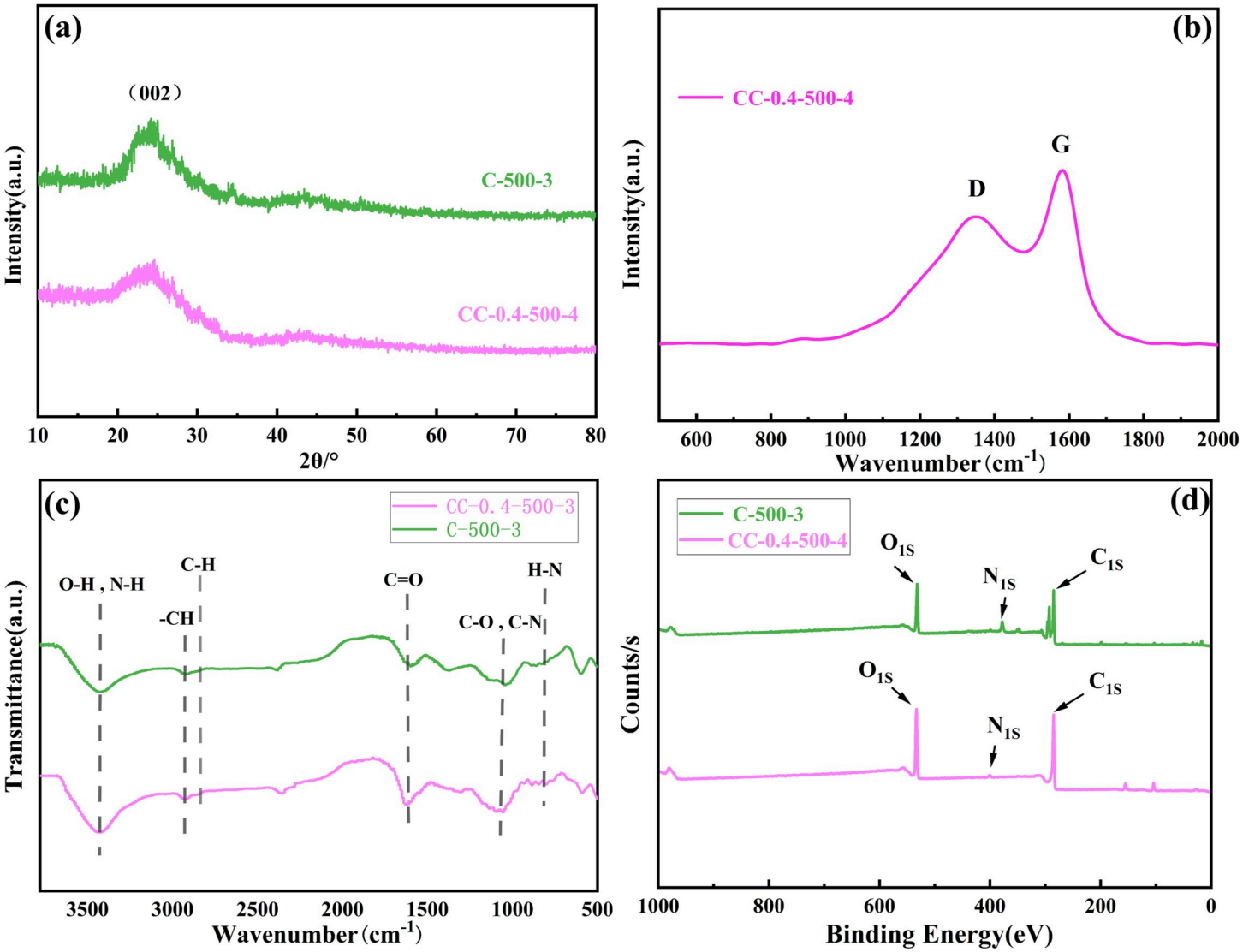

Figure 5

(a) XRD patterns of pristine and oxalic acid-modified biochars; (b) Raman spectrum of oxalic acid-modified biochar; (c) FT-IR spectra of pristine and oxalic acid-modified biochars; and (d) XPS survey spectra of pristine and oxalic acid-modified biochars.

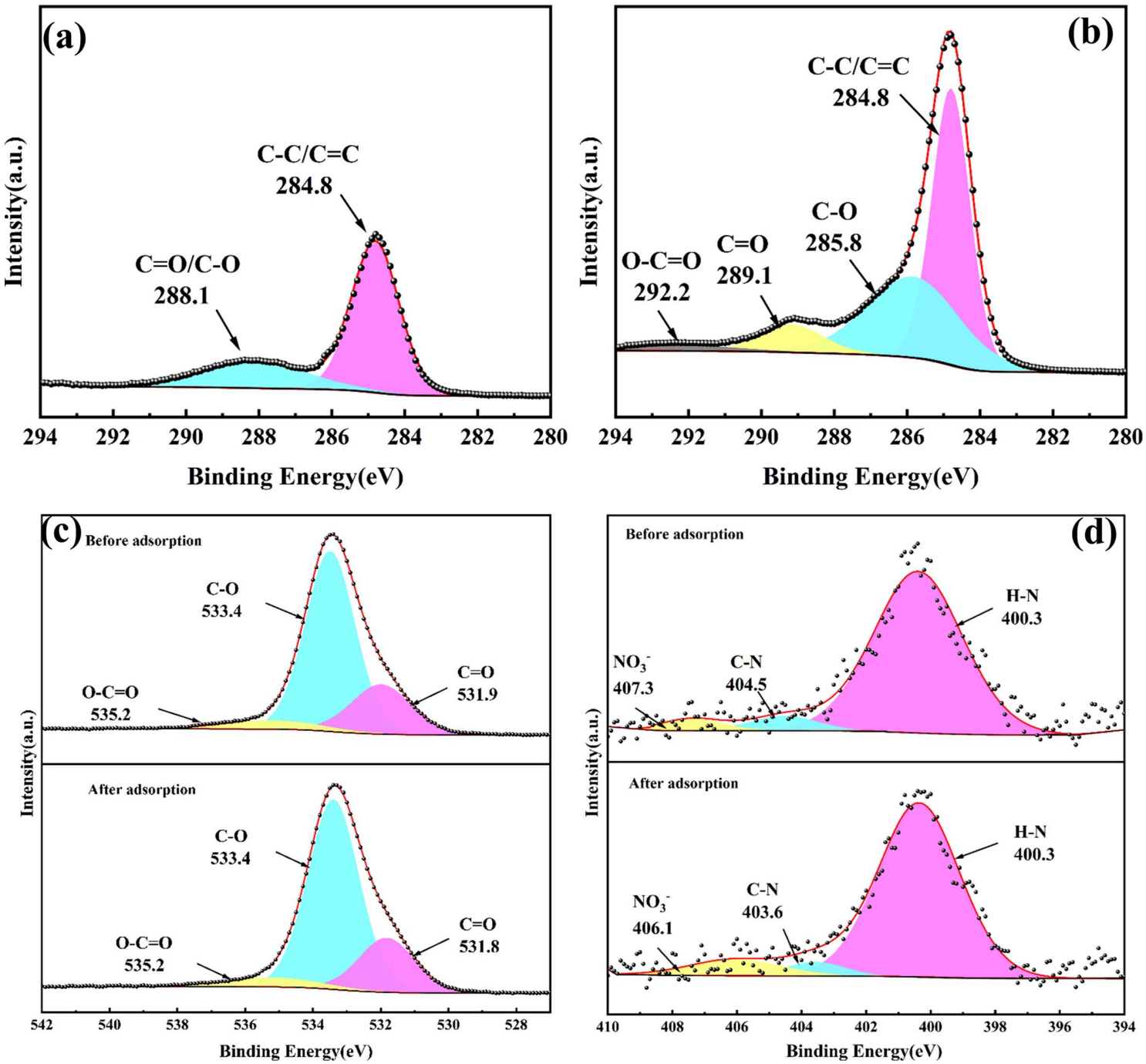

Figure 6

XPS spectra: C 1s spectra of (a) pristine C-500-3 and (b) oxalic acid-modified CC-0.4-500-4; (c) O 1s spectra of CC-0.4-500-4 before and after NH_3 adsorption; and (d) N 1s spectra of CC-0.4-500-4 before and after NH_3 adsorption.

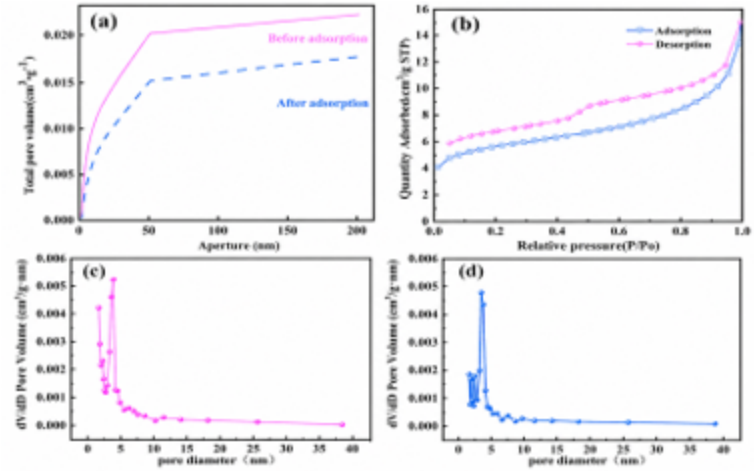

Figure 7

(a) Changes in cumulative pore volume of oxalic acid-modified biochar CC-0.4-500-4 before and after NH_3 adsorption; (b) N_2 adsorption-desorption isotherm of CC-0.4-500-4; and pore-size distributions of CC-0.4-500-4 (c) before and (d) after adsorption.

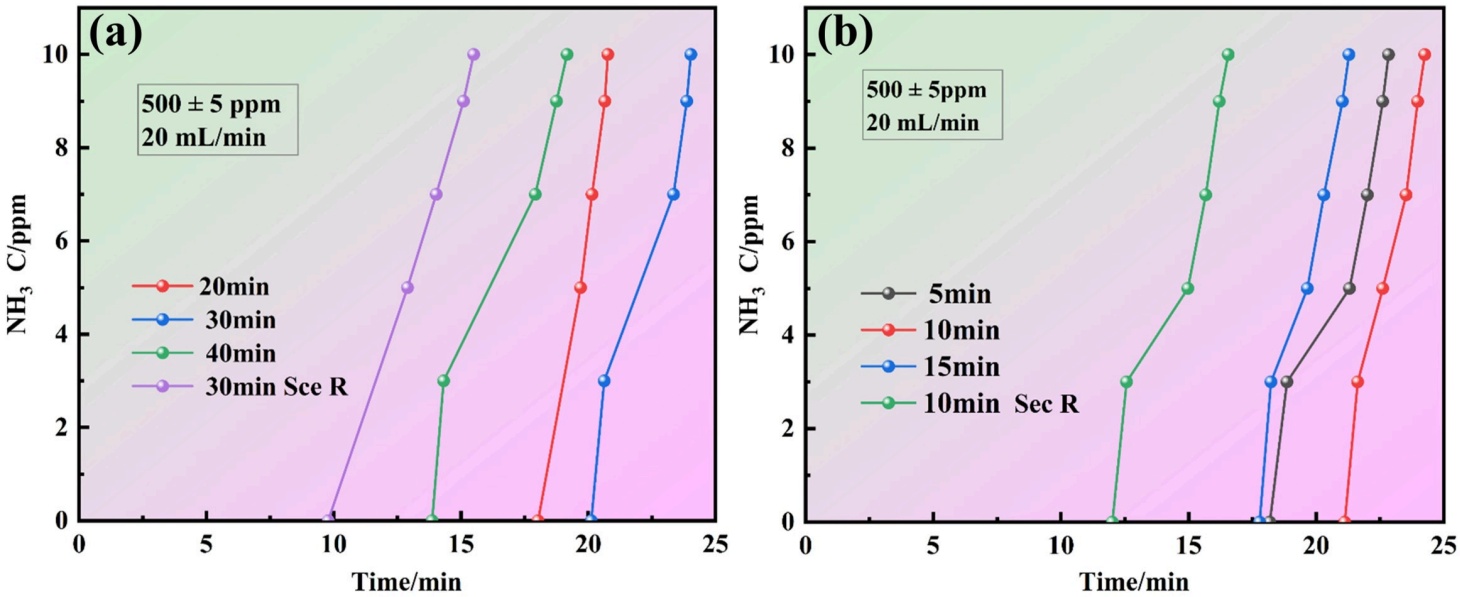

Figure 8

NH_3 adsorption-time profiles of oxalic acid-modified biochar CC-0.4-500-4 after regeneration by (a) water washing for different durations and (b) ethanol washing for different durations.

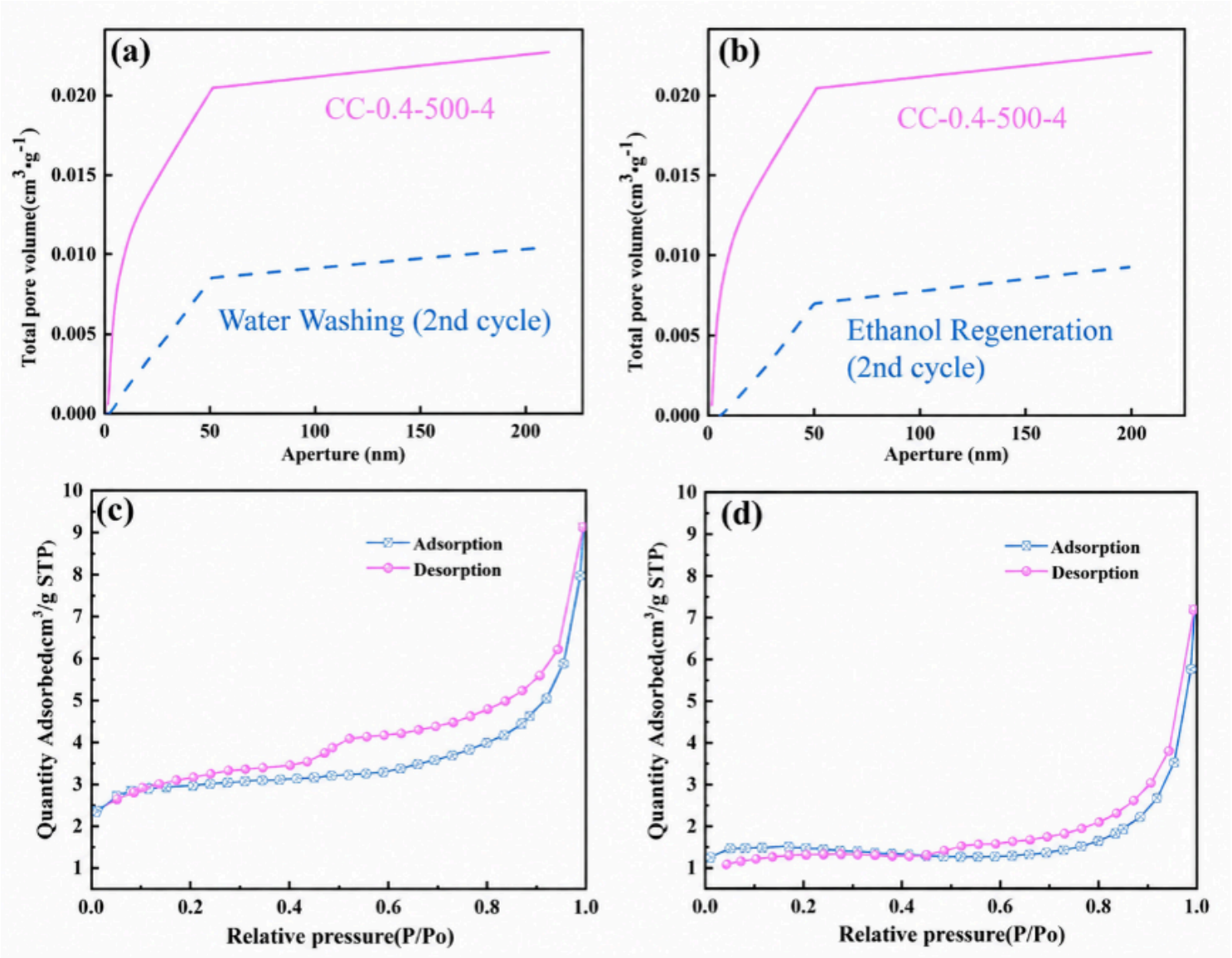

Figure 9

Pore-structure changes and N_2 adsorption-desorption isotherms of oxalic acid-modified biochar CC-0.4-500-4 after two regeneration cycles: cumulative pore volumes of the fresh sample and the sample regenerated twice by (a) water washing and (b) ethanol treatment; N_2 adsorption-desorption isotherms of samples regenerated twice by (c) water washing and (d) ethanol treatment.

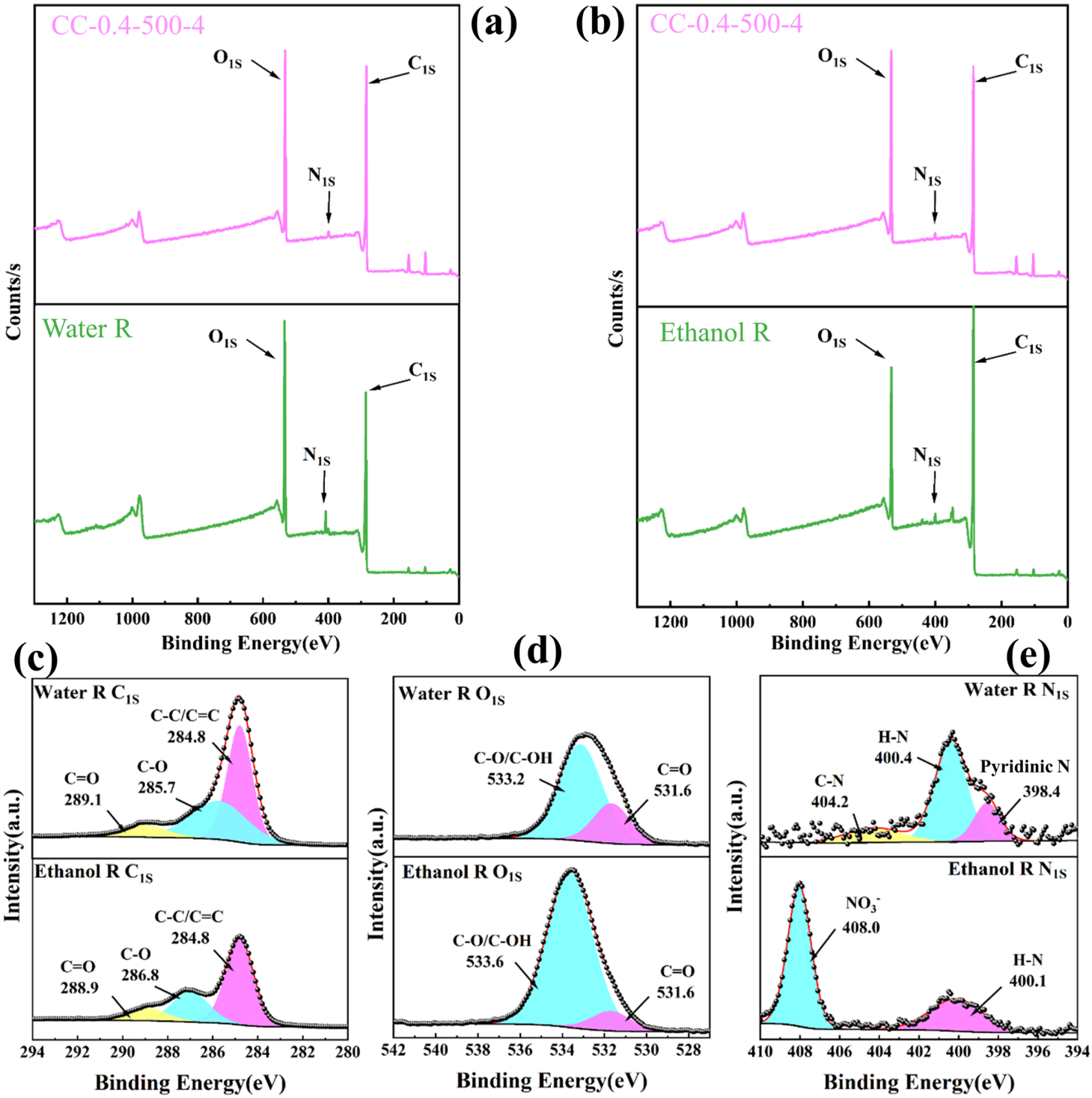

Figure 10

XPS spectra of oxalic acid-modified biochar CC-0.4-500-4 before and after regeneration: survey spectra of the fresh sample and samples regenerated by (a) water washing and (b) ethanol treatment; high-resolution (c) C 1s, (d) O 1s and (e) N 1s spectra of regenerated samples. Water R and Ethanol R denote water-washed and ethanol-regenerated samples, respectively.

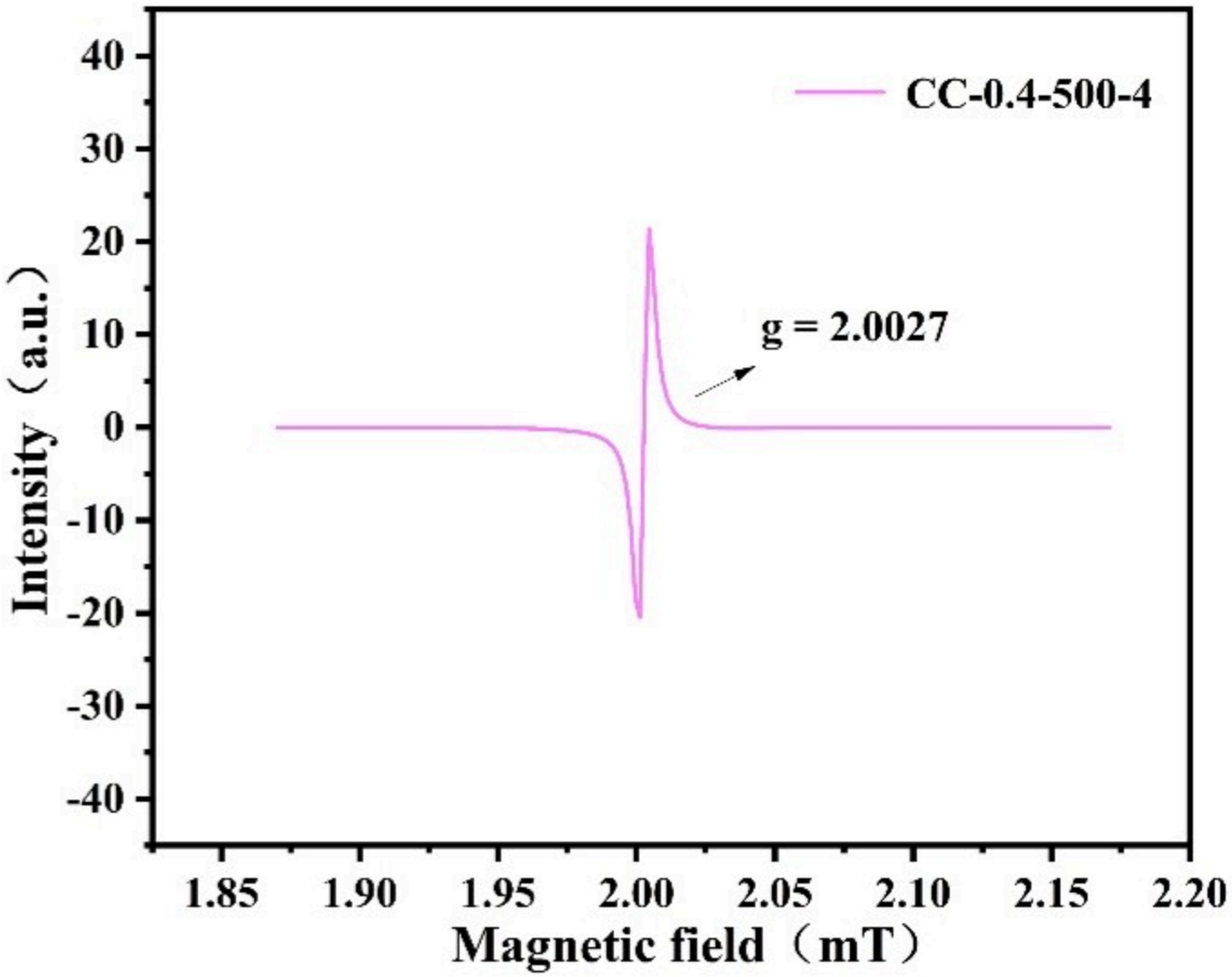

Figure 11

EPR spectrum of persistent free radicals in oxalic acid-modified biochar CC-0.4-500-4.

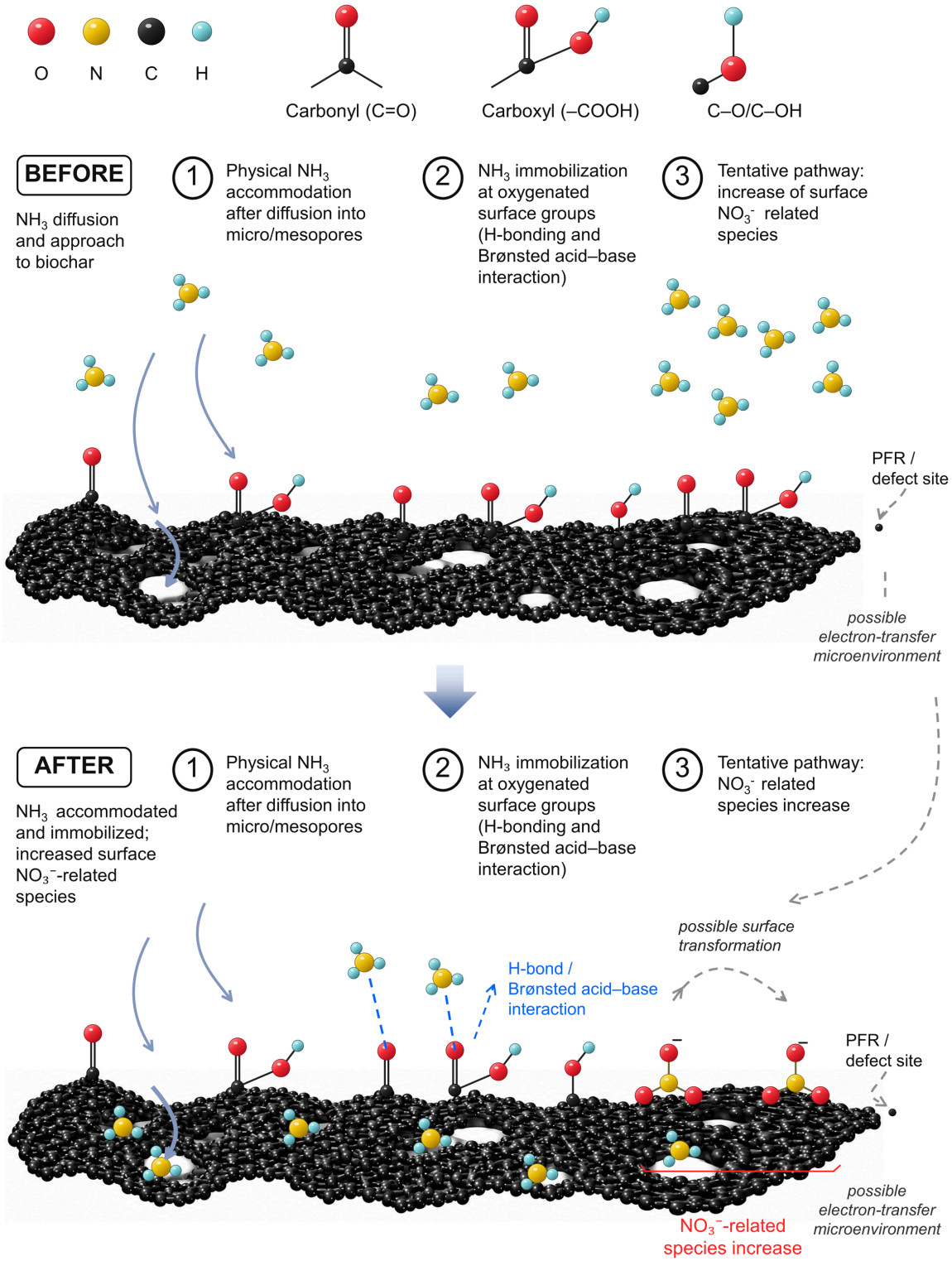

Figure 12

Schematic illustration of the proposed NH_3 adsorption mechanism of oxalic acid-modified biochar.

Supplementary Files

This is a list of supplementary files associated with this preprint. Click to download.

- SupplementaryInformation.docx
- GraphicalAbstract.jpg